This manuscript was accepted by Appl. Phys. Lett. Click here to see the version of record.

Ab initio modeling of steady-state and time-dependent charge transport in hole-only α-NPD devices

Feilong Liu,[1, a)] Andrea Massé,[1] Pascal Friederich,[2] Franz Symalla,[2] Robert Nitsche,[3] Wolfgang Wenzel,[2] Reinder Coehoorn,[1, 4] and Peter A. Bobbert[1]

[1)] *Department of Applied Physics, Eindhoven University of Technology, P.O. Box 513, NL-5600 MB Eindhoven, The Netherlands*

[2)] *Institute of Nanotechnology, Karlsruhe Institute of Technology, D-76344 Eggenstein-Leopoldshafen, Germany*

[3)] *sim4tec GmbH, Arnoldstrasse 18b, D-01307 Dresden, Germany*

[4)] *Institute for Complex Molecular Systems, Eindhoven University of Technology, P.O. Box 513, NL-5600 MB Eindhoven, The Netherlands*

(Dated: 23 November 2016)

We present an *ab initio* modeling study of steady-state and time-dependent charge transport in hole-only devices of the amorphous molecular semiconductor α-NPD. The study is based on microscopic information obtained from atomistic simulations of the morphology and density functional theory calculations of the molecular hole energies, reorganization energies, and transfer integrals. Using stochastic approaches, the microscopic information obtained in simulation boxes at a length scale of $\sim$10 nm is expanded and employed in one-dimensional (1D) and three-dimensional (3D) master-equation modeling of the charge transport at the device scale of $\sim$100 nm. Without any fit parameter, predicted current density-voltage and impedance spectroscopy data obtained with the 3D modeling are in very good agreement with measured data on devices with different α-NPD layer thicknesses in a wide range of temperatures, bias voltages, and frequencies. Similarly good results are obtained with the computationally much more efficient 1D modeling after optimizing a hopping prefactor.

Amorphous organic semiconductors have become important materials for light-emitting diodes, photovoltaic cells, field-effect transistors, and memory devices, because of their advantages over crystalline inorganic semiconductors such as mechanical flexibility, ease of fabrication, and low cost, combined with good performance.[1–4] In order to fully understand the working mechanism of organic devices based on these semiconductors, physically meaningful device models are indispensable. In the past years, many organic device models have been proposed and used by the research community. They can generally be categorized into one-dimensional (1D) and three-dimensional (3D) models. The essential difference between 3D and 1D models is that 3D models include a disordered energy landscape for the charges, while 1D models do not. Therefore, 3D models are able to describe effects such as filamentary currents[5,6] and carrier relaxation.[7] In 3D models, the device is typically modeled as a 3D lattice, and the electrical characteristics are calculated by solving a master equations (ME)[6,7] or by performing kinetic Monte Carlo (KMC) simulations.[8,9] Parameters such as the energetic disorder strength and the hopping rate are required as input. In 1D models, such as 1D drift-diffusion (DD) models,[10–14] the charge-carrier mobility function is required as input.[15,16]

Recently, significant advances have been made towards predicting charge transport in organic semiconductors from *ab initio* calculations at the molecular level.[17–20] However, several questions regarding this *ab initio* approach still remain unanswered: (1) How well do the theoretical predictions of this approach compare to experimental results? (2) How well do 1D modeling results with this approach compare to 3D modeling results? (3) Can this approach predict steady-state as well as time-dependent electrical characteristics?

In this Letter, we show that for hole-only devices based on the amorphous molecular semiconductor α-NPD [N,N′-Di(1-naphthyl)-N,N′-diphenyl-(1,1′-biphenyl)-4,4′-diamine] (molecular structure shown in Fig. 1(a)), *ab initio* modeling yields steady-state current density-voltage ($J(V)$) as well as impedance spectroscopy characteristics that agree very well with experimental results in a wide range of temperatures, bias voltages, and frequencies. We also show that the results of 3D and 1D modeling are very similar. The structure of the investigated devices is shown in Fig. 1(b). They have α-NPD layer thicknesses of $L = 100$ and 200 nm and contain two identical highly p-doped regions that essentially eliminate injection barriers for holes. The $J(V)$ characteristics of these devices have recently been studied by us.[20]

Our *ab initio* modeling starts from a molecular deposition simulation approach described in Ref. 21, yielding an atomistic morphology with a molecular site density $N_t = 0.96 \times 10^{27}$ m^{-3}. Density functional theory (DFT) calculations are performed based on this morphology,[22] yielding the energy distribution of the highest occupied molecular orbital (HOMO), the hole transfer integral distribution, and the hole reorganization energy[23] $E_r = 0.203$ eV. Details of the deposition simulation and the DFT calculations can be found in Refs. 20 and 21. To expand the microscopic information about the morphol-

[a)] Electronic mail: f.liu@tue.nl

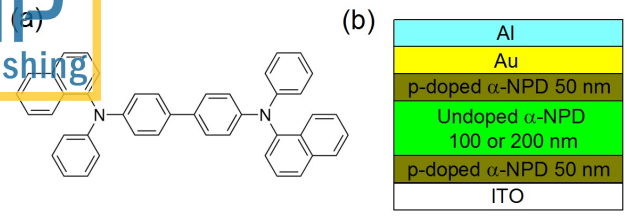

FIG. 1. (a) Molecular structure of α-NPD. (b) Schematic structure of the studied α-NPD devices, with α-NPD layer thicknesses of $L = 100$ and 200 nm. The active area of the devices is $(6.7 \pm 0.7) \times 10^{-6}$ m^2.

ogy and hole transfer integrals obtained in a small simulation box of $10 \times 10 \times 6.5$ nm^3 to an arbitrarily large device simulation box, the same stochastic methods as in Ref. 20 are used.

We note that in Ref. 20 a Gaussian density of states (DOS) of the hole energies was found with a standard deviation $\sigma = 0.130$ eV. In the present work, we have optimized our method for the generation of atomistic morphologies by using instead of the standardized force field in Ref. 20, which tends to underestimate the stiffness of the internal degrees of freedom of the molecules, a material-specific force field. Initial geometry optimizations are performed using DFT as implemented in Turbomole,[24] based on the B3-LYP functional[25] and a def2-SV(P) basis set.[26] Point charges describing the electrostatic potential are obtained using a Mertz-Kollman fit.[27] Dihedral force fields are parameterized using a stepwise rotation and relaxation of the molecular structure around each dihedral angle separately in both directions, where the semi-empirical PM6 method as implemented in MOPAC is used.[28] The dihedral potentials are obtained as the minimum of the two total energy potentials in both rotation directions. This avoids tension and sudden relaxation effects due to steric hindrance. This improved method leads to a lower and more accurate standard deviation of $\sigma = 0.087 \pm 0.003$ eV of the Gaussian hole DOS, in line with a decreased spread in molecular conformations due to the use of the "stiffer" material-specific force field than the standardized force field used in Ref. 20.

We have performed both 3D and 1D device modeling of the electrical characteristics. In our 3D modeling the 3D master equation (ME) is solved for the molecular occupation probabilities for holes, a method that has been applied extensively to model charge transport in amorphous semiconductors.[6,7,15,29] For the devices with highly doped regions studied here, only the undoped region in Fig. 1(b) is explicitly considered. The amorphous α-NPD is modeled by a collection of point sites representing the centers of mass of the molecules and charge transfer integrals between these points, both generated with the stochastic methods described in Ref. 20. It was found in Ref. 20 that the correlation in the HOMO energies of neighboring sites is small and we therefore assume spatially uncorrelated Gaussian energy disorder. Marcus rates are taken for the hopping of holes between the sites.[20]

The highly p-doped regions are treated as metallic electrodes with zero injection/extraction barrier, which means that we put the Fermi energy of the electrodes at the center of the Gaussian hole DOS in the α-NPD. We note that the details of the injection and collection process are not important for the final results, because the current is space charge-limited and not injection-limited. We implement these electrodes in the 3D ME calculations as 2D square arrays of sites with a lattice constant of 1 nm, placed at a distance of 0.5 nm from the box where the α-NPD sites are generated, where each site can always inject or collect a hole. We refer to Ref. 6 for further details about the introduction of electrode sites in this way.

For the calculation of $J(V)$ characteristics the 3D ME is solved in a similar way as in Ref. 6. In impedance spectroscopy, in addition to a dc bias V a small bias $\Delta V(t) = \Delta V \exp(2\pi \mathrm{i} f t)$ is applied with a frequency f. The frequency dependent complex impedance $Z(f)$ is defined as the zero-amplitude limiting value of the ratio of $\Delta V(t)$ and the response $\Delta I(t)$ in the current. Calculations of $Z(f)$ both within the 3D and 1D ME framework start with the steady-state solution corresponding to the dc bias V, followed by a linearization in ΔV. In the case of the 3D ME calculations this linearization procedure is explained in Ref. 7. In the case of the 1D ME calculations a similar procedure is followed.[30] The 3D ME calculations are typically performed with boxes containing around 10^6 molecules, followed by an average over five different random energy disorder realizations.

In the 1D ME calculations the α-NPD is modeled as a chain of discrete sites at the typical intermolecular distance of 1 nm. Intersite hopping rates are taken that are consistent with the temperature and carrier density dependence of the mobility, which is obtained from Ref. 15. The advantage of 1D ME over 1D DD calculations is that the electric field dependence of the mobility is taken into account implicitly.[31] We checked that, with the same parameters, the 1D ME calculations provide essentially the same $J(V)$ curves as the 1D DD calculations in Ref. 20.

The measured and modeled $J(V)$ characteristics of devices with α-NPD layer thicknesses $L = 100$ and 200 nm at three different temperatures are shown in Fig. 2. We find that the 3D ME predictions show very good agreement with the experimental results. We stress that *these calculations do not contain a single adjustable parameter*. In particular, we use exactly the same value $\sigma = 0.087$ eV for the standard deviation of the Gaussian hole DOS as obtained from the *ab initio* calculations. By contrast, in Ref. 20 the value $\sigma = 0.130$ eV found with a standardized force field had to be adjusted to $\sigma = 0.10$ eV to obtain agreement with experiment. We note that we improved our device modeling with respect to Ref. 20 in two ways. (1) A series resistance $R_S = 50\ \Omega$ present in the experimental measurement setup that was neglected in Ref. 20 is now included. The effect of this series re-

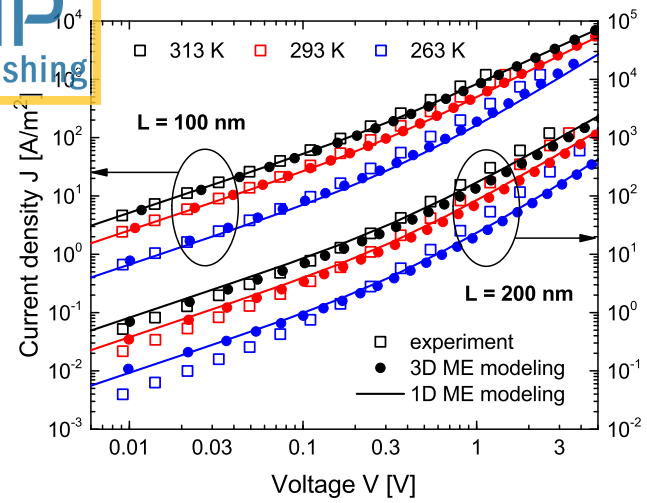

FIG. 2. Current density-voltage, $J(V)$, characteristics at three different temperatures for devices with the structure given in Fig. 1(b), with α-NPD layer thicknesses of $L = 100$ and 200 nm. Open squares: experimental data. Closed circles: 3D ME results. Lines: 1D ME results.

sistance is clearly seen in the impedance spectroscopy measurement discussed below. (2) The relative dielectric constant ε_r of α-NPD has been changed from the value $\varepsilon_r = 3.8$ taken in Ref. 20 to the value $\varepsilon_r = 3.0$, which also follows from the impedance spectroscopy measurements. Both improvements lead with the value $\sigma = 0.087$ eV to a better agreement between predictions and measurements.

By only optimizing one hopping rate prefactor, which is temperature-independent, we find that the 1D ME results for the $J(V)$ curves essentially reproduce the 3D ME results (full curves in Fig. 2). We therefore conclude that the 1D ME calculations, which are much faster than the 3D ME calculations, are sufficient in this case to obtain the temperature dependence and shape of the $J(V)$ curves. This can be understood from the fact that percolation effects, which can only be captured by a 3D approach, are unimportant when the organic layer thickness is much larger than the characteristic length scale of percolation.[6,32] The mobility function used in the 1D ME calculations yields a room-temperature hole mobility of 2×10^{-8} m^2/Vs for α-NPD in the limit of vanishing carrier concentration and electric field. This is considerably larger than the value of 2.9×10^{-9} m^2/Vs reported in Ref. 20 and much closer to the value of 3×10^{-8} m^2/Vs found in time-of-flight (TOF) experiments.[33] Hence, the discrepancy discussed in Ref. 20 between the hole mobility extracted from the $J(V)$ modeling and that obtained from TOF experiments is also largely resolved. We note that the dependence of the mobility on the electric field extracted from our modeling is not of the Poole-Frenkel type. A parametrization of the field dependence was given in Ref. 20, which for the case of α-NPD was found to be very close to that found in Ref. 15. Because of the limited field range for which TOF experiments are usually performed, it is hard to distinguish different models for the field dependence of the mobility.

Although the agreement between the predicted and measured $J(V)$ curves is good, it is still not excellent. The measured $J(V)$ curves are, in particular at low temperatures, steeper than the modeled ones. This underestimation of the field dependence could be due to the neglected weak spatial correlation in the energetic disorder[16,20] or to a small amount of traps.

The real and imaginary parts of the measured and modeled impedance, $\mathrm{Re}(Z(f))$ and $\mathrm{Im}(Z(f))$, respectively, as a function of frequency f at the three different temperatures T and at different dc bias voltages V are shown in Fig. 3 for the two devices. In the low-frequency limit, the values of $\mathrm{Re}(Z)$ for different V and T are consistent with the $J(V)$ data in Fig. 2. In the high-frequency limit, all curves of $\mathrm{Re}(Z)$ converge to 50 Ω, which is attributed to a series resistance in the indium tin oxide (ITO) bottom contact of the devices; see Fig. 1(b). This resistance has been taken into account both in the modeling of the $Z(f)$ curves and the $J(V)$ curves in Fig. 2. In the high-frequency limit, all curves of $-\mathrm{Im}(Z)$ converge to $(2\pi f C_{\mathrm{geo}})^{-1}$, where C_{geo} is the geometric capacitance of the device. From the value of C_{geo}, the value of the relative dielectric constant $\varepsilon_r = 3.0$ is obtained, which is also used in the $J(V)$ modeling. The frequency where $-\mathrm{Im}(Z)$ is maximal and where the drop in $\mathrm{Re}(Z)$ occurs can be interpreted as the RC time of the device. In accordance with this interpretation this frequency increases with increasing V and T, because the conductivity of the devices then increases, as is clear from Fig. 2.

The results in Fig. 3 show that the agreement of both the 3D and 1D ME $Z(f)$ results with the experimental results is, just like in the case of the $J(V)$ results, in general very satisfactory. For the device with $L = 200$ nm larger deviations are observed than for the device with $L = 100$ nm, as in the case of the $J(V)$ results. The explanation for these deviations is very likely the same as in the case of the $J(V)$ modeling. Slight differences between the 3D and 1D ME results are observed, in particular for $\mathrm{Im}(Z)$ at high V and low f. These differences could be related to carrier relaxation effects. In principle, such effects are taken into account in a better way in 3D calculations. In a recent impedance spectroscopy study of devices of a polyfluorene-based organic semiconductor large differences were observed between 3D ME and 1D DD calculations at frequencies below 10^3 Hz, where a much better modeling was obtained with the 3D ME calculations.[7] In the present study, we cannot make a similar comparison, because the experimental signal-to-noise ratio rapidly decreases below 10^3 Hz.

In conclusion, we have shown that it is possible to describe the steady-state and time-dependent charge transport properties of hole-only devices of the important organic semiconductor α-NPD, using as input only microscopic information from *ab initio* morphology simulations and DFT calculations. Without adjusting a single pa-

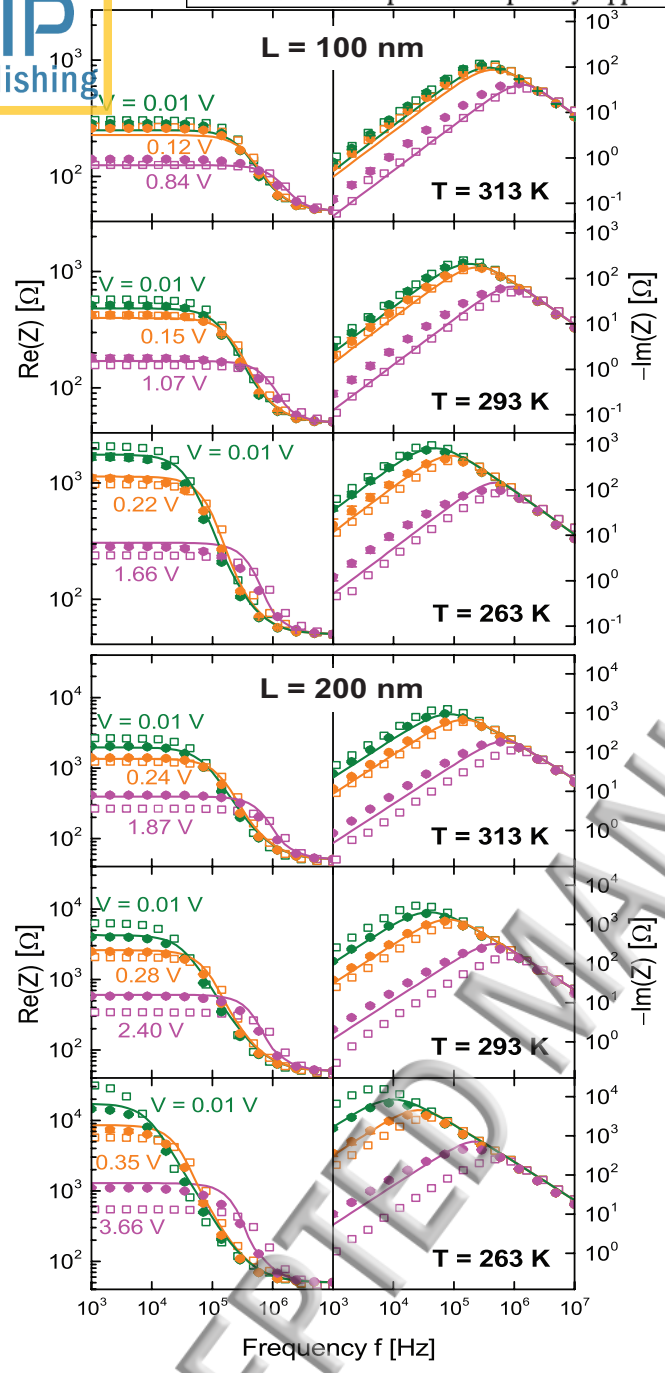

FIG. 3. Real and imaginary parts of the impedance Z as a function of frequency f at different temperatures and bias voltages for the α-NPD device with $L = 100$ nm (upper panels) and $L = 200$ nm (lower panels). Open symbols: experimental data. Closed symbols: 3D ME results. Lines: 1D ME results.

rameter, very good agreement with experiment is obtained by solving a 3D master equation for the full device. In particular, the standard deviation σ of the energy disorder is a critical parameter. By using an improved force field as compared to previous work[20] we obtain a value of σ that can readily be used in the modeling of the temperature dependent current density-voltage characteristics and impedance spectroscopy data. Good results are also obtained in a computationally more efficient way by solving a 1D master equation, which requires the optimization of a hopping prefactor.

This research is part of the Horizon 2020 EU projects EXTMOS (contract No. 646176) and MOSTOPHOS (contract No. 646259), of the German project "UNiverselles Verständnis der Defekte in Materialien für die flexible ELektronik" (UNVEiL), funded by the German Federal Ministry of Education and Research (BMBF), and of the Dutch-German project "Modeling of organic light-emitting diodes: From molecule to device" (MODEOLED), funded on the Dutch side by the Dutch Technology Foundation (STW; Project No. 12200), which is part of the Dutch Science Foundation (NWO), and on the German side by the "Deutsche Forschungsgemeinschaft" (DFG; Project No. WE1863/22-1). The *ab initio* morphology and DFT calculations were performed on the computational resource ForHLR Phase I, funded by the German Ministry of Science, Research and the Arts Baden-Württemberg, and the DFG. We thank Dr. S. L. M. van Mensfoort and Dr. H. van Eersel from Simbeyond B.V. for stimulating discussions.

[1] J. H. Burroughes, D. D. C. Bradley, A. R. Brown, R. N. Marks, K. Mackay, R. H. Friend, P. L. Burns, and A. B. Holmes, Nature **347**, 539 (1990).
[2] C. W. Tang, Appl. Phys. Lett. **48**, 183 (1986).
[3] G. Horowitz, Adv. Mater. **10**, 365 (1998).
[4] P. Heremans, G. H. Gelinck, R. Müller, K. Baeg, D. Kim, and Y. Noh, Chem. Mater. **23**, 341 (2011).
[5] M. Cölle, M. Büchel, D. M. de Leeuw, Org. Electron. **7**, 305 (2006).
[6] J. J. M. van der Holst, M. A. Uijttewaal, R. Balasubramanian, R. Coehoorn, P. A. Bobbert, G. A. de Wijs, and R. A. de Groot, Phys. Rev. B **79**, 085203 (2009).
[7] M. Mesta, J. Cottaar, R. Coehoorn, and P. A. Bobbert, Appl. Phys. Lett. **104**, 213301 (2014).
[8] H. Bässler, Phys. Stat. Sol. (b) **175**, 15 (1993).
[9] M. Mesta, M. Carvelli, R. J. de Vries, H. van Eersel, J. J. M. van der Holst, M. Schober, M. Furno, B. Lüssem, K. Leo, P. Loebl, R. Coehoorn, and P. A. Bobbert, Nat. Mater. **12**, 652 (2013).
[10] J. S. Bonham and D. H. Jarvis, Aust. J. Chem. **31**, 2103 (1978).
[11] P. S. Davids, I. H. Campbell, and D. L. Smith, J. Appl. Phys. **82**, 6319 (1997).
[12] S. L. M. Mensfoort and R. Coehoorn, Phys. Rev. B **78**, 085207 (2008).
[13] E. Knapp. R. Häusermann, H. U. Schwarzenbach, and B. Ruhstaller, J. Appl. Phys. **108**, 054504 (2010).
[14] F. Liu, P. P. Ruden, I. H. Campbell, and D. L. Smith, J. Appl. Phys. **111**, 094507 (2012).
[15] W. F. Pasveer, J. Cottaar, C. Tanase, R. Coehoorn, P. A. Bobbert, P. W. M. Blom, D. M. de Leeuw, and M. A. J. Michels, Phys. Rev. Lett. **94**, 206601 (2005).
[16] M. Bouhassoune, S. L. M. van Mensfoort, P. A. Bobbert, and R. Coehoorn, Org. Electron. **10**, 437 (2009).
[17] P. Kordt, J. J. M. van der Holst, M. Al Helwi, W. Kowalsky, F. May, A. Badinski, C. Lennartz, and D. Andrienko, Adv. Funct. Mater. **25**, 1955 (2015).
[18] L. Wang, G. Nan, X. Yang, Q. Peng, Q. Li, and Z. Shuai, Chem. Soc. Rev. **39**, 423 (2010).
[19] P. Friederich, V. Meded, A. Poschlad, T. Neumann, V. Rodin, V. Stehr, F. Symalla, D. Danilov, G. Lüdemann, R. F. Fink, I. Kondov, F. von Wrochem, and W. Wenzel, Adv. Funct. Mater. **26**, 5757 (2016).

[20] A. Massé, P. Friederich, F. Symalla, F. Liu, R. Nitsche, R. Coehoorn, W. Wenzel, and P. A. Bobbert, Phys. Rev. B **93**, 195209 (2016).
[21] T. Neumann, D. Danilov, C. Lennartz, and W. Wenzel, J. Comput. Chem. **34**, 2716 (2013).
[22] P. Friederich, F. Symalla, V. Meded, T. Neumann, and W. Wenzel, J. Chem. Theory Comput. **10**, 3720 (2014).
[23] V. Coropceanu, J. Comil, D. A. da Silva Filho, Y. Olivier, R. Silbey, and J.-L. Brédas, Chem. Rev. **107**, 926 (2007).
[24] R. Ahlrichs, M. Bär, M. Häser, H. Horn, and C. Kölmel, Chem. Phys. Lett. **162**, 165 (1989).
[25] A. D. Becke, J. Chem. Phys. **98**, 1372 (1993).
[26] A. Schäfer, H. Horn, and R. Ahlrichs, J. Chem. Phys. **97**, 2571 (1992).
[27] U. C. Singh and P. A. Kollman, J. Comput. Chem. **5**, 129 (1984).
[28] J. J. P. Stewart, Stewart Computational Chemistry - MOPAC, see http://openmopac.net/.
[29] Z. G. Yu, D. L. Smith, A. Saxena, R. L. Martin, and A. R. Bishop, Phys. Rev. B **63**, 085202 (2001).
[30] W. C. Germs, S. L. M. van Mensfoort, R. J. de Vries, and R. Coehoorn, J. Appl. Phys. **111**, 074506 (2012).
[31] R. Coehoorn and S. L. M. van Mensfoort, Phys. Rev. B **80**, 085302 (2009).
[32] A. Massé, R. Coehoorn, and P. A. Bobbert, Phys. Rev. Lett. **113**, 116604 (2014).
[33] C. H. Cheung, K. K. Tsung, K. C. Kwok, and S. K. So, Appl. Phys. Lett. **93**, 083307 (2008).

(a)

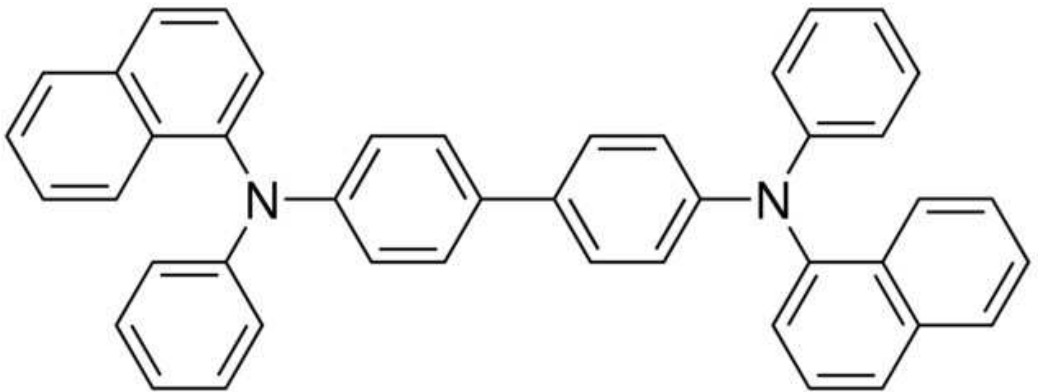
N
N

(b)

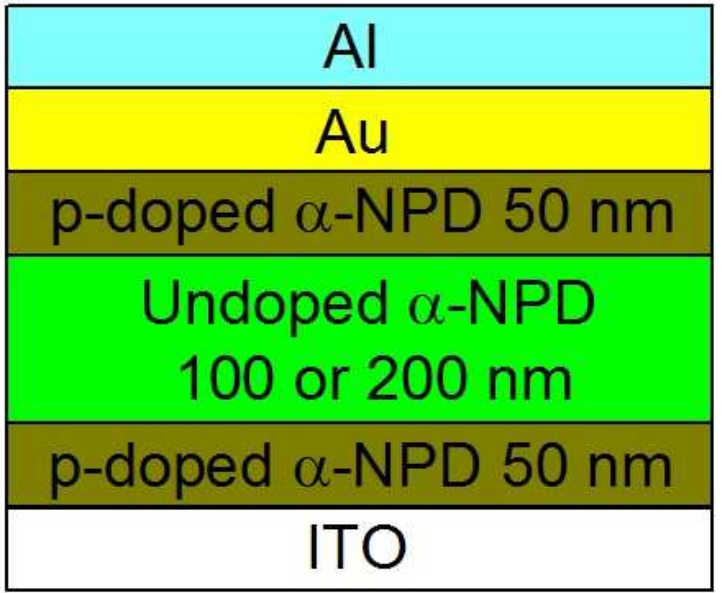
Al
Au
p-doped α-NPD 50 nm
Undoped α-NPD
100 or 200 nm
p-doped α-NPD 50 nm
ITO

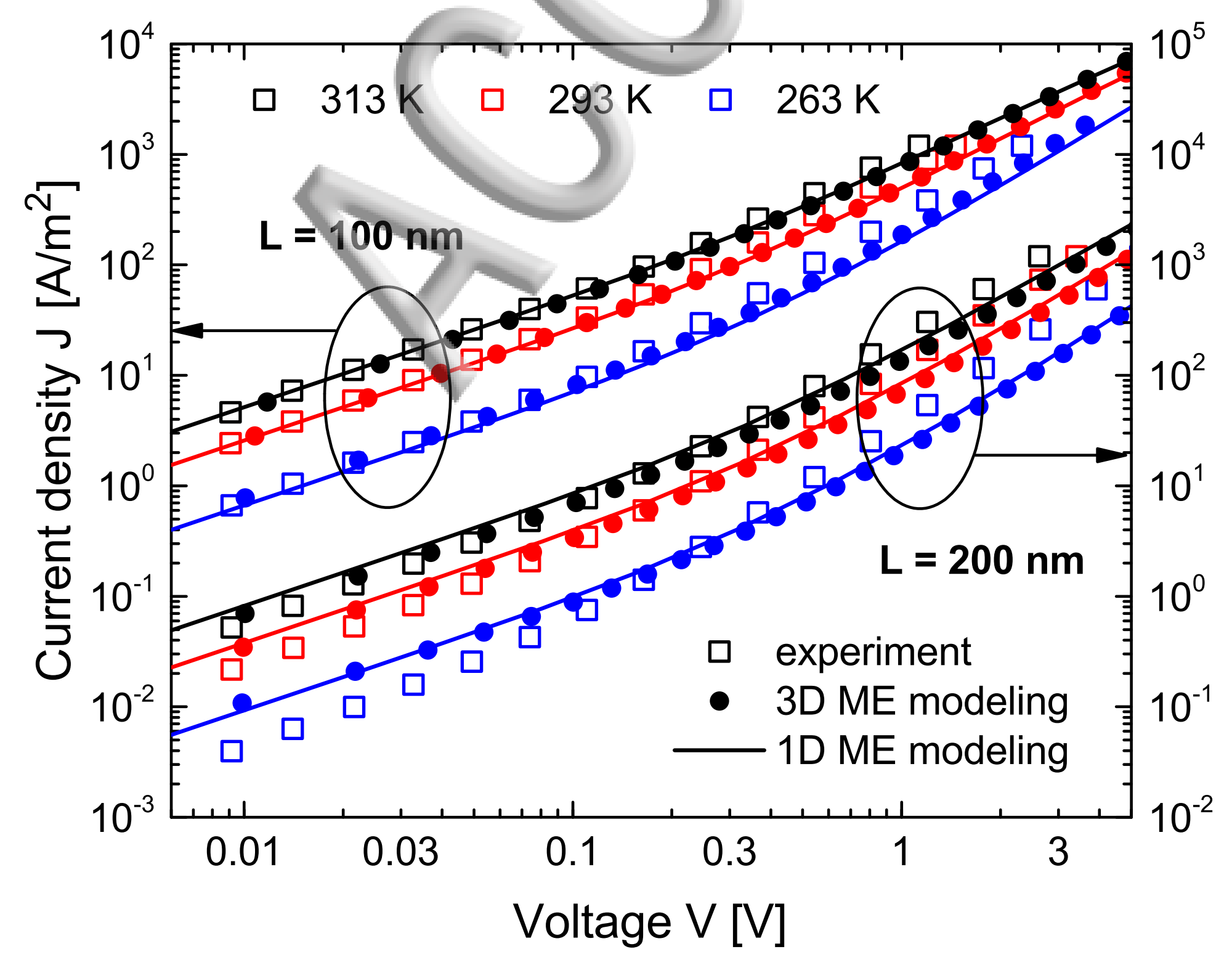
313 K
293 K
263 K
L = 100 nm
L = 200 nm
experiment
3D ME modeling
1D ME modeling
Current density J [A/m^2]
Voltage V [V]
10^{4}
10^{3}
10^{2}
10^{1}
10^{0}
10^{-1}
10^{-2}
10^{-3}
10^{5}
10^{4}
10^{3}
10^{2}
10^{1}
10^{0}
10^{-1}
10^{-2}
0.01
0.03
0.1
0.3
1
3

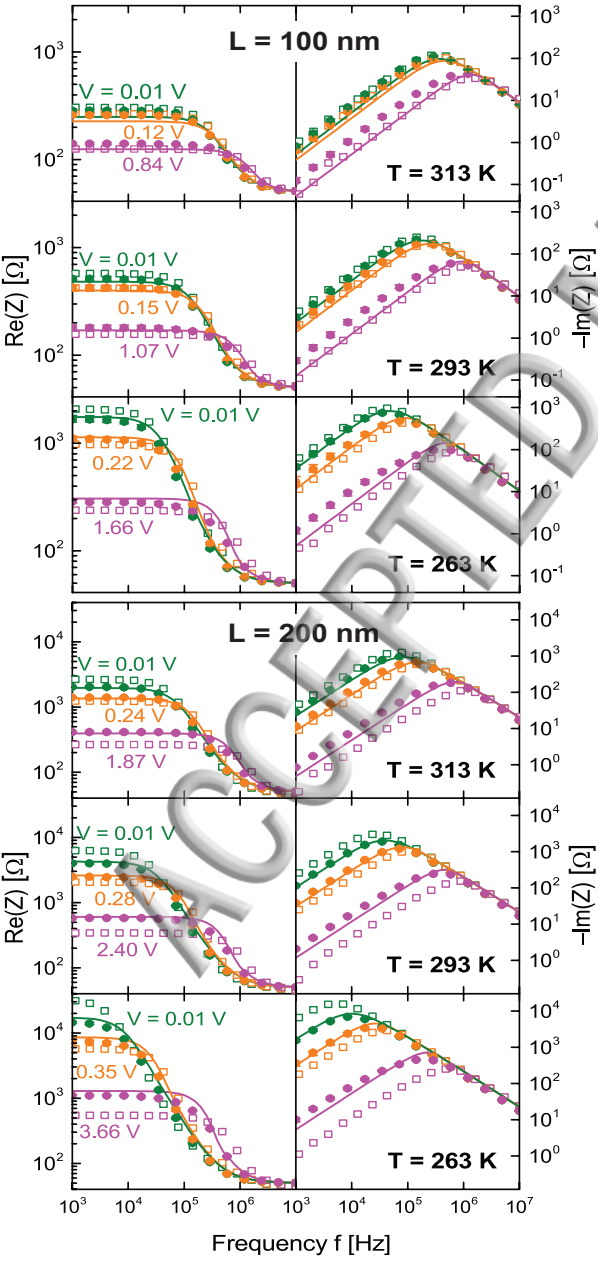
L = 100 nm
V = 0.01 V
0.12 V
0.84 V
T = 313 K
V = 0.01 V
0.15 V
1.07 V
T = 293 K
V = 0.01 V
0.22 V
1.66 V
T = 263 K
L = 200 nm
V = 0.01 V
0.24 V
1.87 V
T = 313 K
V = 0.01 V
0.28 V
2.40 V
T = 293 K
V = 0.01 V
0.35 V
3.66 V
T = 263 K
Re(Z) [Ω]
−Im(Z) [Ω]
Frequency f [Hz]